Dropsizing of Near-Nozzle Diesel and RME Sprays by Microscopic Imaging

C. Crua*, G. de Sercey, M. R. Heikal
Centre for Automotive Engineering, University of Brighton, UK
C.Crua@brighton.ac.uk, G.DeSercey@brighton.ac.uk and M.R.Heikal@brighton.ac.uk

M. Gold
BP Global Fuels Technology, Pangbourne, UK
Martin.Gold@uk.bp.com

Abstract

The morphological composition of a typical modern Diesel spray is known to include complex structures such as ligaments and amorphous droplets, but most laser dropsizing techniques cannot diagnose drops that deviate from the spherical shape. Whilst direct imaging has potential for resolving arbitrary shapes, challenges remain to measure microscopic droplets in dense sprays. To this end, progress made with ongoing experimental investigations of the atomisation of diesel and biodiesel fuels is reported for the near-nozzle region using a long working distance microscope. The light source and imaging optics were optimised to produce blur-free shadowgraphic images of sprays with a viewing region of 593x784 µm. A number of image processing techniques were explored and described to identify both small and large liquid structures. A discrete wavelet transform was found to improve the detection of droplets smaller than 10 µm, and contrast-limited adaptive histogram equalisation provided the best detection of medium droplets and large ligaments. The measured diameters were compensated based on an analysis of the droplets' local contrast and size. Droplet size distributions were measured for a non-additised diesel fuel and rape-methyl ester. The image processing algorithm was found to successfully discriminate between the two fuels.

Introduction

The experimental characterization of the initial stage of diesel jet formation and primary breakup under realistic engine conditions is challenging due to the harsh environment in which they take place. This inherent complexity is compounded by the highly transient nature of the processes involved, along with the elevated velocities and the microscopic scale at which they occur. The small size and high velocities of the droplets produced through the primary and secondary breakup have made their direct visualisation particularly difficult. Hence the characterisation of these microscopic and fast droplets has been almost exclusively conducted indirectly by observing their interaction with incident laser beams. Techniques based on the Doppler effect (LDA, PDA) have been particularly popular, although novel laser diagnostics are being actively developed such as interferometric imaging (ILIDS) and rainbow refractometry. These techniques can potentially measure the droplets diameters with a high level of accuracy, but they are fundamentally unable to characterise non-spherical droplets and ligaments. The morphological composition of a typical Diesel spray is known to include structures such as ligaments, amorphous and spherical droplets but, as shown in Figure 1, the quantity of fuel occupied by perfectly spherical droplets can represent a relatively small proportion of the total injected volume. Hence the data obtained through these diagnostic techniques provide a partial and biased characterisation of the spray. Indeed, the need to extend optical droplet characterisation to non-spherical shapes was highlighted in the recent review by Tropea [1].

Microscopic imaging experiments of diesel sprays have been reported in the literature (e.g. [2-7]), although with varying degrees in the quality of the images produced. Satisfactory lighting can be particularly difficult to obtain at microscopic level. High-power short duration laser pulses may seem appropriate, but speckle patterns caused by the combined reflections of such monochromatic light conceal the underlying morphology of the spray, thus significantly degrading the quality of the resulting images and making their interpretation limited. Such optical artifacts can be observed in images recorded by Lai et al. [5], Badock et al. [4] and Heimgärtner & Leipertz [2], for example. Speckle patterns can be avoided by using a spark light instead of a laser, but the duration of the spark flashes are significantly longer and lead to motion blurring, even at low spray velocities, unless the exposure can be accurately controlled by the imaging device. The relatively long and random jitter associated with the timing of the spark can also lead to a significant proportion of 'missed' acquisitions which, combined with the long recharge time of the high-voltage electronics, may significantly lengthen the experimental work.

* Corresponding author

An additional issue associated with still imaging is the inherent lack of information on the spatiotemporal evolution of the transient jet and droplets observed. Specifically, there is no information on the velocity field, a quantity which is of particular significance for the investigation of breakup and essential for the approximation of relevant parameters such as the Weber and Reynolds numbers.

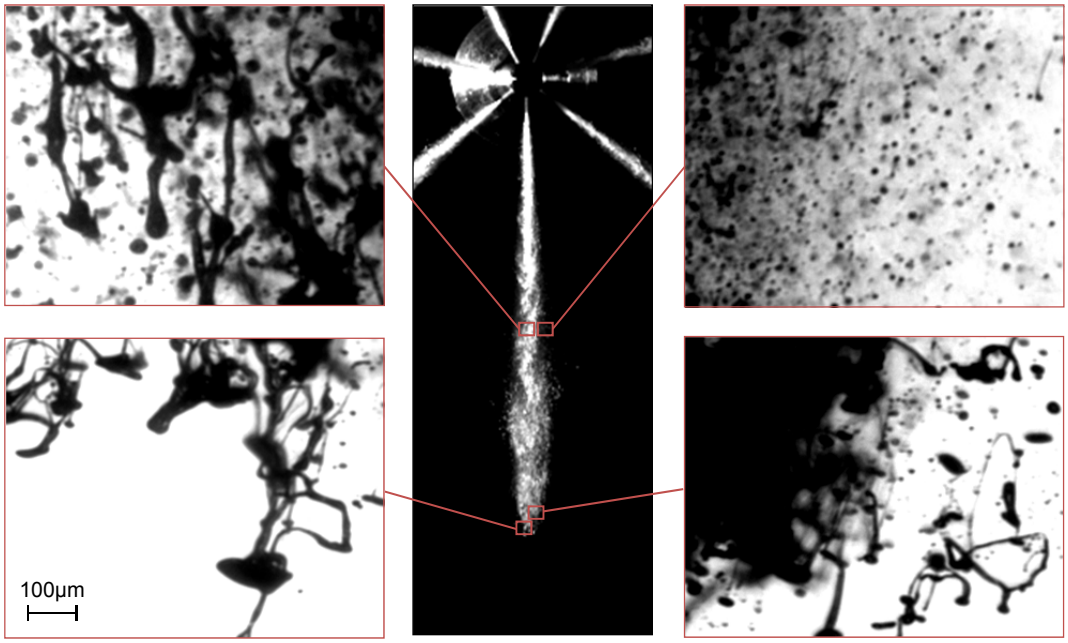

Figure 1 Shadowgraphs of non-additised fossil diesel sprays with sub-micron resolution, and their approximate locations shown on a side-lit spray. Injection at 40 MPa into atmospheric conditions.

In the present work, progress made with ongoing experimental investigations of the atomisation of diesel and biodiesel fuels is reported for the near-nozzle region using a long working distance microscope. High quality shadowgraphic photographs of diesel sprays were obtained by spectrally diffusing a high-power laser pulse. These still images provided high resolution blur-free observations of the injection process at a microscopic scale, at the nozzle exit and in several locations where secondary breakup is expected to occur.

Experimental Methods

Experimental setup

The experiment was performed in a static enclosure at atmospheric conditions. The fuel was delivered by a Delphi common-rail system, comprising a DFP-3 high-pressure pump rated at 200 MPa, and a seven-hole DFI-1.3 injector with a VCO type nozzle. The nozzle's orifices were cylindrical with a diameter of 135 µm and a length/diameter ratio of 8. The nozzle had an equivalent cone angle of 154°. The injector was mounted orthogonally relative to the camera, as shown in Figure 2, and rotated so that the imaged spray propagated downwards in the chamber. A detailed description of the test rig is covered by Crua [8].

The optical setup was covered in detail by the authors in [9], hence only the main features are included here. The light source was a frequency-doubled Nd:YAG laser, with a pulse duration of 7 ns. The light pulse was spectrally diffused and spatially expanded from 8 mm to 100 mm to provide homogeneous illumination over a sufficiently large area. A high performance dual-frame camera with a Peltier-cooled 12 bit CCD sensor was fitted with a long range microscope. The optics were selected to obtain a magnification factor of 10.8 at the CCD sensor plane. Hence the resolution was 0.57 µm per pixel and the viewing region was 593x784 µm. The main experimental conditions for the images presented in this paper are listed in Table 1. A total of 200 images was recorded for each test point. Although velocimetry is not the focus of this paper, the use of a double-pulsed light source combined with a dual-frame camera and an interframe time of 400 ns allowed capturing the displacement of the atomised fuel, as well as the droplet size distribution.

Table 1. Experimental conditions for droplet sizing. Timings are relative to start of injection trigger.

Injection pressure	100 MPa
Nozzle orifice diameter	135 μm
Gas pressure	1 atm
Axial distance from nozzle	10; 15 mm
Radial distance from axis	300 μm
Acquisition timings	670; 695 μs
Image resolution	0.57 μm per pixel
Image size	593x784 μm

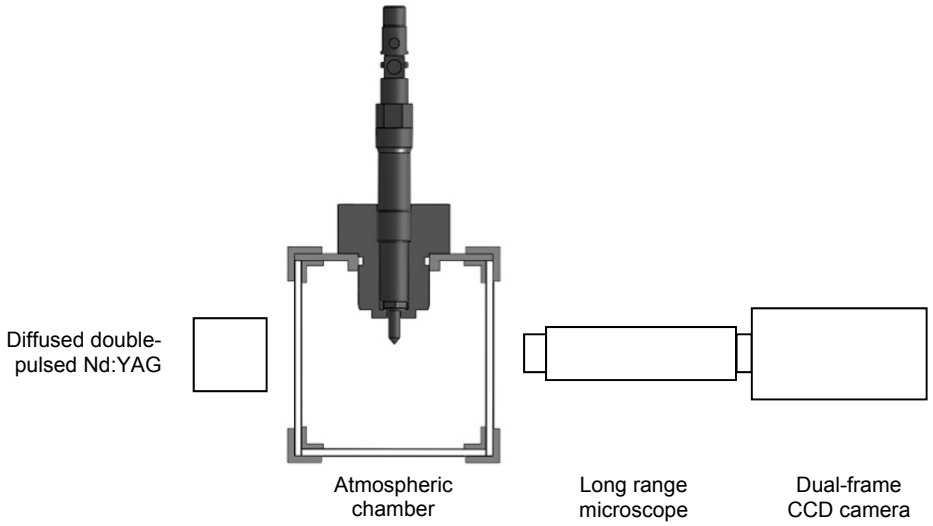

Figure 2 Optical setup for the microscopic imaging of diesel sprays.

Fuel samples

Two fuels with different physical properties were selected, and their properties listed in Table 2. The diesel fuel was a non-additised ultra low sulphur petroleum diesel. Rape methyl ester (RME) was chosen for its higher density, viscosity and surface tension compared to fossil diesel, which are expected to lead to larger droplets.

Table 2. Physical properties of fuels tested

Property	**Fossil Diesel**	**RME**
Density at 15°C ($kg.m^{-3}$)	837	883
Kinematic viscosity ($mm^2.s^{-1}$)	3.3	4.4
Surface tension ($dyn.cm^{-1}$)	29.8	33.2

Droplet Sizing and Discussion

The main attribute of the dropsizing algorithm is that it can compensate for the blurring and lack of contrast of droplets due to their very small size or their position relative to the focus plane. Blaisot and Yon [10] showed that the ratio between the droplet's real and measured sizes is a function solely depending on the local contrast of that droplet. The local contrast of a droplet was obtained using the Michelson contrast, defined as:

$$C = \frac{I_{max} - I_{min}}{I_{max} + I_{min}} \tag{1}$$

where I_{max} is the maximum of the droplet's background intensity and I_{min} the minimum of the droplet's intensity. In the present work, the relationship between droplet size ratio and droplet contrast was established using a NIST calibrated dot target, of nominal diameters ranging from 1.9 to 102 µm. In order to simulate a change in contrast the dots were translated along the focus plane and images of these dots were recorded under the exact same optical conditions as the experiment. The calibrated dots' size and contrast were then measured using the dropsizing algorithm described below and the size ratio plotted against contrast. The relation between droplet size ratio and droplet contrast was fitted by a 4th order polynomial function (Figure 3).

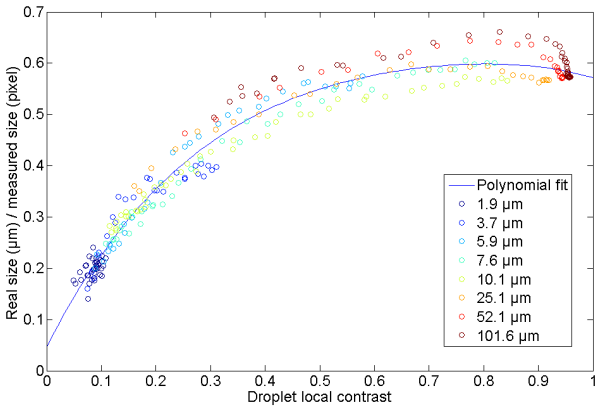

Figure 3 Size ratio as a function of local contrast for a range of calibrated dot diameters.

Droplet detection algorithms

In order to compensate for non-homogeneities in the illumination source, the raw images were normalised by a white image. The white images consisted of an image of the scene illuminated by the laser without any spray. To account for shot-to-shot variations in laser energy, 20 white images were recorded and averaged for each test point. The camera used for the experiment had a Peltier-cooled sensor which produced very low thermal noise, hence a dark current correction was not found to be necessary.

The dropsizing algorithm incorporates 3 main steps: droplet detection, droplet sizing, and contrast-based size compensation. The objective of the droplet detection is to transform the greyscale image into a binary image, where white pixels indicate a droplet and black pixels indicate the background. Each connected group of pixel in the binary image can then be labelised as a single droplet. The requirement of the droplet detection algorithm is to detect a maximum number of droplets whilst minimizing false positives. This can become rather challenging in the case of dense polydisperse sprays, where droplet contrast varies significantly with droplet diameter. A combination of several detection algorithms is essential to appropriately capture the full droplet size distribution. The following droplet detection methods were investigated and assessed in isolation:

1. Constant thresholding: With this method, the image is binarised using a constant threshold intensity below which all pixels are set to one and above which all pixels are set to zero. The use of a constant threshold indicates an assumption that the background intensity is constant over the whole image, and that the droplets shadow intensities are always significantly below that of the background. However, the background intensity is not always constant, particularly near the liquid core of the spray where it may be reduced by liquid absorption of the light. Additionally, the droplets shadow intensities may not always be significantly below that of the background, particularly for polydisperse sprays with small droplet diameters. An example of constant thresholding is shown in Figure 5, where it can be observed that large ligaments are over-detected and the smaller droplets missed.

2. Intensity range thresholding: This method is similar to the constant thresholding method except that the threshold level is a fixed percentage of the entire image's intensity range. As a result, this technique can be use-

ful to compensate for shot-to-shot energy variations. Nevertheless, it suffers from the same issues as the basic thresholding method.

3. Wavelet transform: This binarisation method is explained in more detailed in [10]. It consists in applying a linear convolution between the image and a 'mexican-hat' type wavelet (Figure 4) with an equation of the form $\frac{1}{r^2} e^{-r^2/2}$. The result is an image that highlights the concavity (2nd derivative) of the intensity gradient of circular objects of the same scale as the wavelet. The image resulting from this transformation is then binarised using intensity range thresholding. The wavelet transform method is particularly efficient at detecting small circular droplets (Figure 5), regardless of their contrast with the background [11]. However, larger amorphous structures cannot be detected by the wavelet transform, as evident in Figure 5.

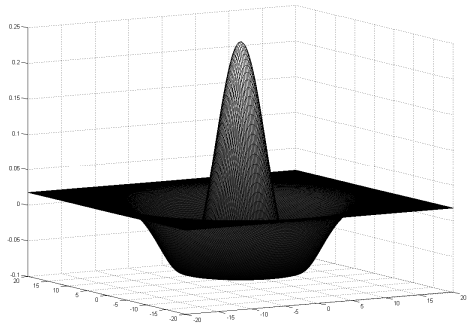

Figure 4 Typical mexican-hat wavelet

4. Background adaptive thresholding: The purpose of this method is to locally adjust the threshold level used by the constant thresholding method according to the average intensity around each pixel. For this, the image is smoothed using a Gaussian blur of a radius large enough to eliminate any feature (such as individual droplets) from the image. The blurred image, multiplied by a constant threshold value, is then used to binarise the original image. The crucial part of this technique is the tuning of the blur radius. However, a single blur radius that could apply to the range of droplet density and sizes found in diesel sprays could not found.

5. Contrast-Limited Adaptive Histogram Equalisation (CLAHE) thresholding: Following on the idea of technique 4 of using an adaptive threshold, the CLAHE method uses local histogram equalization to enhance the contrast of local features in the image [12]. The equalised image is then binarised using the constant thresholding technique. Due to the adaptive equalisation, this technique was effective at detecting droplets near the core of the spray. One weakness of the technique is that it also enhances fine structures of the spray core that are then mistaken as droplets. As these structures are usually an order of magnitude larger than most droplets they can be ignored during later stages. It can be observed in Figure 5 that the CLAHE method correctly detects large and medium sized structures in the original image, but misses low-contrast features such as the smaller droplets.

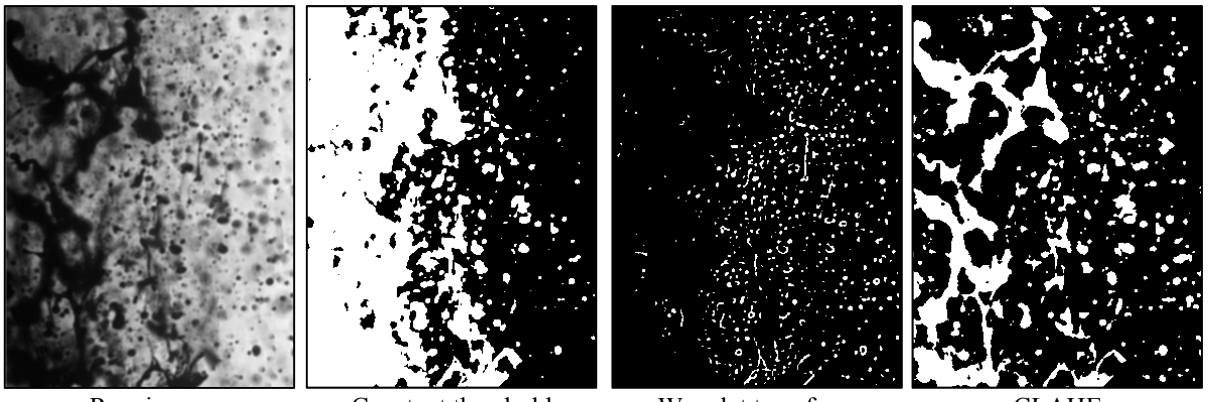

Raw image | Constant threshold | Wavelet transform | CLAHE

Figure 5 Original raw image (593x784 µm) recorded at 10 mm from the nozzle of a diesel spray injected at 40 MPa, and binary images obtained using the constant, wavelet, and CLAHE methods.

It is evident from Figure 5 that no detection method successfully identified all the droplets present in the original image. The small droplets were best detected by the discrete wavelet transform, whilst medium droplets and large ligaments were best identified by the contrast-limited adaptive histogram equalization method. There-

fore both methods were used in the droplet detection algorithm. The wavelet transform image and CLAHE image were both computed and then combined into a single binary image. All clusters of orthogonally connected pixels within the binary image were then detected to produce a labelised image.

Droplet sizing

This second phase of the dropsizing algorithm is concerned with measuring the droplets' equivalent diameters. It takes as input the original image and the labelised image generated by the previous step. The algorithm iterates over each labelised cluster of pixels using the binary image of the cluster as a mask in the original image. Clusters near the edge of the image are ignored to avoid capturing partial droplets. The mask is first dilated to three times its original area and any pixel corresponding to a different label, i.e. a different droplet is then removed from the mask. The final mask is then used to isolate the droplet's image and background from the full image, but with any neighbouring droplet removed. The projected surface area of the droplet is then measured using intensity range thresholding (method 2 above). The equivalent diameter d is calculated from the surface A as $d = 2\sqrt{A/\pi}$.

The final phase of the image processing algorithm converts the measured droplet size in pixel to a droplet size in micrometers, based on the droplet's local contrast. Each droplet's local contrast is measured using Equation (1), and the corrected droplet size is obtained by multiplying the measured size by the calibration polynomial (Figure 3) for that contrast.

Comparison between diesel and RME

We compared the morphology of diesel and RME jets observed at the nozzle exit using microscopic imaging and ultra-high-speed video in [13]. The focus of the present discussion will be on the extraction of droplet sizes from the shadowgraphic micrographs. Examples of such images are included in Figure 6, including the initial jet at the nozzle exit and sample images recorded at 10 and 15 mm from the orifice for 100 MPa injection pressures.

Figure 6 confirms that droplet density is high and structures larger than 10 µm can be significantly deformed. Dropsizing techniques based on the Doppler effect, interferometry or refractometry would be unable to provide statistically significant measurements in these regions. Multiple scattering, beam steering and amorphous structures would invalidate most measurements [14], introducing a bias towards spherical and isolated droplets. Shadowgraphic micrographs have other limitations (e.g. diffraction limit) but they may yield measurements in locations normally inaccessible by other dropsizing techniques.

Droplet size distributions for the non-additised diesel fuel and RME are shown in Figure 7 with 0.5 µm bins. Both the probability density (left axes) and the cumulative distribution (right axes) functions are shown for the diesel and RME fuels at 2 locations downstream of the nozzle. A total of 200 images were recorded for each test point. The number of detected droplets for each test point were between 106 758 and 133 718, giving an average of 600 droplets per image. Since the viewing region was 0.465 mm^2 we can estimate the average droplet density at 1 300 drops/mm^2. By taking into account the depth of field of the imaging system (20 µm) the volumetric droplet density can be estimated at 65 000 drops/mm^3.

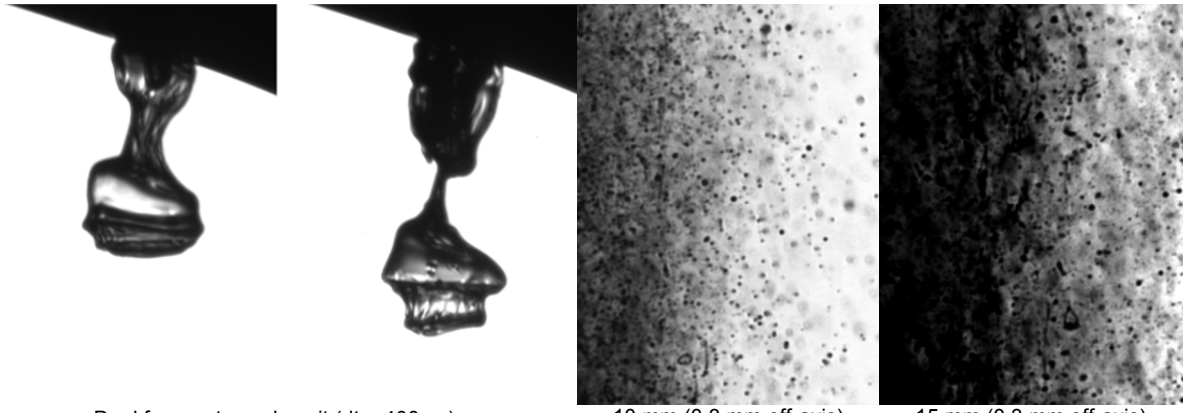

Figure 6 Examples of shadowgraphic micrographs recorded for RME at 3 locations. The left edge of images recorded downstream from the nozzle (100 MPa pressure) is 0.3 mm from the spray axis.

It is interesting to note that the droplet size distributions in Figure 7 peak at 2 µm, even though the measurements were conducted under non-evaporating conditions. This can be attributed to secondary atomization already being underway. The distributions in Figure 7(a) indicate that at 10 mm away from the nozzle differences between the atomization properties of the diesel and RME were captured by the image processing. As ex-

pected from the physical properties of the selected fuels, the size distributions indicate that the RME produced a higher number of larger droplets than the non-additised petroleum diesel. The size distributions recorded for the 10 mm position intersect at the 8 µm bin, and the effect of the fuels' physical properties appear to only have a small influence on droplet sizes. Figure 7(b) shows that for the 15 mm position the intersection of the droplet size distributions occurred at the 5 µm bin. The differences between the distributions are more pronounced with the RME's being more skewed to the right than the diesel's. This is again consistent with the expectation that the atomization of RME is inhibited by its higher viscosity and surface tension.

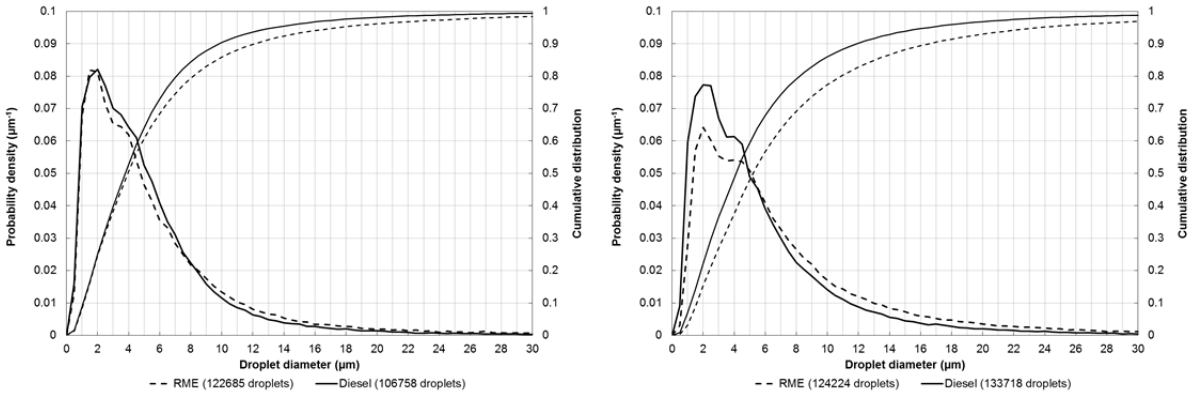

(a) 10 mm from nozzle exit (b) 15 mm from nozzle exit

Figure 7 Droplet size distributions recorded 10 mm (left) and 15 mm (right) below the nozzle exit for RME and diesel sprays injected at 100 MPa. The number of droplets measured are indicated in brackets.

Applicability of the technique to high pressure and temperature environments

The focus of this paper is on the development of a sizing method that can yield information in the near-nozzle region without requiring droplet sphericity. Whilst this initial implementation justifies a simplified experimental setup, it is important to consider the applicability of the method at realistic engine conditions. Firstly, typical peak pressures and temperatures in modern Diesel engines should lead to transcritical thermodynamic conditions. The injected fuel is supercritical with respect to pressure, and is likely to transition from subcritical to supercritical with respect to temperature. This is expected to lead to a reduction, and ultimately a disappearance, of surface tension and latent heat of vaporization. We can expect that droplets located in the colder regions of the spray will have a less well-defined interface than the images shown in Figures 1 and 6. Fuel located in the hotter regions of the spray should rapidly diffuse with the surrounding gas, with no distinct droplet boundary. In both cases, optical diagnostics that rely on scattering (e.g. Doppler techniques) or refraction (e.g. rainbow refractometry and ILIDS) will yield little data, biased towards transcritical spherical droplets, or no data at all. The light intensity in shadowgraphs is linked to the second spatial derivative of the refractive index. Thus shadowgraphic micrographs can theoretically yield information for both the liquid and vapour phases of the injected fuel.

Additional complications introduced in high pressure and temperature environments include the presence of turbulence, density and temperature gradients in the gas phase, which will result in refractive index fluctuations. We can expect 2D Doppler techniques to be at a significant disadvantage due to their requirement for the precise intersection of five optical paths: four lasers and one receiving optic. Microscopic shadowgraphy requires two aligned optical paths: one for the imaging, and one for the bulk collimated illumination. The image quality is sensitive to the geometrical alignment of these two paths, but the technique can tolerate imperfect alignments.

We conducted tests on a reciprocating rapid compression machine to evaluate the applicability of microscopic shadowgraphy for dropsizing in high pressure and temperature environments. A detailed description of the test rig is covered by Crua in [8] and [9]. The peak motored pressure was 6 MPa and peak temperature estimated at 850 K. The injection equipment, fuel and optical configuration were the same as those described for the dropsizing tests conducted at atmospheric conditions. Sample images recorded at the nozzle exit and 7 mm from the orifice are shown in Figure 8. The dual frame images recorded at the nozzle exit confirm that deformed liquid droplets exist and can be visualized by shadowgraphic microscopy. They also show mild intensity gradients at the tip of the liquid spray, indicating the presence of vaporized fuel. Interestingly, droplets can be visualised 7 mm from the orifice but their interfaces are distinctly less clear than at atmospheric conditions (Figure 6). This could be due to the droplets approaching supercritical conditions, or refractive index fluctuations degrading the shadowgraphs. Although the quality of the shadowgraphic micrographs is reduced, both qualitative and quantitative information on droplet size, shape and velocity can be extracted from such images. We should emphasize that approximately 80% of the images recorded at elevated pressure conditions were significantly degraded, most

likely due to steering of the optical paths by refractive index gradients. This supports our statement that diagnostics requiring the intersection of multiple optical paths are less likely to succeed in such conditions.

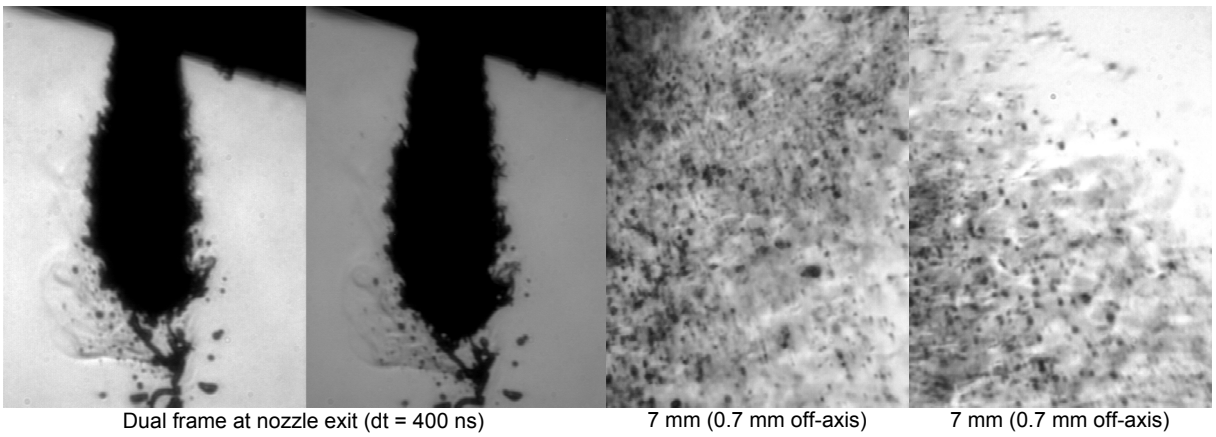

Figure 8 Examples of shadowgraphic micrographs recorded for Diesel fuel injected at 40 MPa into gas at 6 MPa pressure and 850 K temperature.

Summary and Conclusions

Progress made with ongoing experimental investigations of the atomisation of diesel and biodiesel fuels were reported for the near-nozzle region. Shadowgraphic micrographs were found to yield measurements in locations normally inaccessible by other dropsizing techniques. A number of image processing techniques were explored and described. A discrete wavelet transform was used to improve the detection of small droplets and contrast-limited adaptive histogram equalisation was used to detect medium and large droplets. Droplet size distributions were produced at 10 mm and 15 mm below the nozzle exit for RME and diesel sprays injected at 100 MPa. The image processing algorithm was found to successfully discriminate between the two fuels.

There is a wide scope for future works, both on the development of the technique and its application to elevated in-cylinder pressures and temperatures.

Acknowledgements

This work was supported by BP International Ltd (GF&LT); and the UK's Engineering and Physical Science Research Council [Industrial CASE grant number 07000437]. The authors are grateful to Dr T. Shoba and Mr J. Ratinaud for their assistance with the experiment, and the EPSRC Engineering Instrument Pool for the loan of equipment used for this study.

References

[1] Tropea, C., *Annual Review of Fluid Mechanics* 43:399-426 (2011).
[2] Heimgartner, C., Leipertz, A., *8th ICLASS*, Pasadena, USA, July, pp. 1235-1241.
[3] Bae, C., Yu, J., Kang, J., Kong, J., Lee, K.O., *SAE 2002-01-1625*(2002).
[4] Badock, C., Wirth, R., Fath, A., Leipertz, A., *International Journal of Heat and Fluid Flow* 20:538-544 (1999).
[5] Lai, M., Wang, T., Xie, X., Han, J., Henein, N., Schwarz, E., Bryzik, W., *SAE transactions* 107:1283-1293 (1998).
[6] Sjöberg, H., Manneberg, G., Cronhjort, A., *Optical Engineering* 35:3591 (1996).
[7] Badock, C., Wirth, R., Fath, A., Leipertz, A., *International Journal of Heat and Fluid Flow 20(5)*538-544 (1999).
[8] Crua, C., "Combustion Processes in a Diesel Engine," School of Engineering, University of Brighton, Brighton, 2002.
[9] Crua, C., Shoba, T., Heikal, M.R., Gold, M.R., Higham, C., *SAE paper 2010-01-2247*, 25-27 October.
[10] Blaisot, J., Yon, J., *Experiments in Fluids* 39:977-994 (2005).
[11] González-Nuevo, J., Argüeso, F., López-Caniego, M., Toffolatti, L., Sanz, J.L., Vielva, P., Herranz, D., *Monthly Notices of the Royal Astronomical Society* 369:1603-1610 (2006).
[12] Zuiderveld, K., *Graphics gems IV*, pp. 474-485: Academic Press Professional, 1994.
[13] Shoba, T., Crua, C., Heikal, M.R., Gold, M.R., *24th ILASS-Europe*, Estoril, Portugal, 5-7 September.
[14] Lacoste, J., Crua, C., Heikal, M.R., Kennaird, D., Gold, M.R., "PDA characterization of dense diesel sprays using a common-rail injection system."